

LETTER TO THE EDITOR

Near-infrared spectropolarimetry of a δ -spot

H. Balthasar¹, C. Beck², R. E. Louis¹, M. Verma^{1,3}, and C. Denker¹

¹ Leibniz-Institut für Astrophysik Potsdam (AIP), An der Sternwarte 16, 14482 Potsdam, Germany
e-mail: hbalthasar@aip.de

² National Solar Observatory/Sacramento Peak, P.O. Box 62, Sunspot, NM 88349, U.S.A.

³ Max-Planck-Institut für Sonnensystemforschung, Max-Planck-Straße 2, 37191 Katlenburg-Lindau, Germany

Received January 23, 2020; accepted MMMM DD, YYYY

ABSTRACT

Sunspots harboring umbrae of both magnetic polarities within a common penumbra (δ -spots) are often but not always related to flares. We present first near-infrared (NIR) observations (Fe I $\lambda 1078.3$ nm and Si I $\lambda 1078.6$ nm spectra) obtained with the Tenerife Infrared Polarimeter (TIP) at the Vacuum Tower Telescope (VTT) in Tenerife on 2012 June 17, which afford accurate and sensitive diagnostics to scrutinize the complex fields along the magnetic neutral line of a δ -spot within active region NOAA 11504. We examine the vector magnetic field, line-of-sight (LOS) velocities, and horizontal proper motions of this rather inactive δ -spot. We find a smooth transition of the magnetic vector field from the main umbra to that of opposite polarity (δ -umbra), but a discontinuity of the horizontal magnetic field at some distance from the δ -umbra on the polarity inversion line. The magnetic field decreases faster with height by a factor of two above the δ -umbra. The latter is surrounded by its own Evershed flow. The Evershed flow coming from the main umbra ends at a line dividing the spot into two parts. This line is marked by the occurrence of central emission in the Ca II $\lambda 854.2$ nm line. Along this line, high chromospheric LOS-velocities of both signs appear. We detect a shear flow within the horizontal flux transport velocities parallel to the dividing line.

Key words. Sun: sunspots – Sun: magnetic field – Sun: photosphere – Sun: chromosphere – Techniques: polarimetric

1. Introduction

In some cases, a sunspot penumbra contains umbrae of opposite magnetic polarities as first described by Künzel (1960). A few years later, Künzel (1965) introduced the new category ‘ δ -spot’ extending Hale’s spot classification in terms of the magnetic field. Although δ -spots are frequent and often associated with flares (see Sammis et al. 2000), accurate measurements of the magnetic field vector with high resolution are still rare, especially in the NIR. In the context of flares and δ -spots, observations beyond $1 \mu\text{m}$ have been limited to white-light flare emission at $1.56 \mu\text{m}$ after major X-class flares (e.g., Xu et al. 2004, 2006) and sporadic long-wavelength infrared spectropolarimetry in the Mg I $\lambda 12.32 \mu\text{m}$ line (e.g., Jennings et al. 2002).

Velocity investigations in the visible are more frequent. Persistent downflows of up to 14 km s^{-1} within the penumbra close to the polarity inversion line (PIL) have been reported by Martínez Pillet et al. (1994). At lower spectral and spatial resolution, similar downflows of $1.5\text{--}1.7 \text{ km s}^{-1}$ have been detected by Takizawa et al. (2012) in regions of penumbral decay. Evershed flows of opposite polarity umbrae converge near the PIL and have to pass each other, which is indicative of an interleaved system of magnetic field lines (Lites et al. 2002; Hinzberger et al. 2009). Moreover, significant up- and downflows in excess of 10 km s^{-1} are encountered during flares (Fischer et al. 2012).

The observed δ -spot shares a remarkable visual resemblance with its counterpart in the flare-prolific active region NOAA 10930, which by contrast exhibits significant rotation (up to $8^\circ \text{ hour}^{-1}$) of the δ -umbra (Min & Chae 2009). Shear flows along the PIL potentially contribute to the build-up of non-potential magnetic field configurations (cf., Denker et al. 2007).

Conversely, Tan et al. (2009) note that the shear flow between opposite polarity umbrae decreases from 0.6 km s^{-1} before to 0.3 km s^{-1} after an X3.4 flare.

In this Letter, we introduce NIR spectropolarimetry as a diagnostic tool to study the intriguing properties of δ -spots.

2. Observations

On 2012 June 17, not far from the maximum of the solar cycle No. 24, we observed a sunspot with a δ -configuration in active region NOAA 11504 at 18° S and 29° W ($\mu = \cos \vartheta = 0.82$). A map of the full Stokes vector was obtained with the Tenerife Infrared Polarimeter (TIP; Collados et al. 2007) and adaptive optics’ correction (Berkefeld et al. 2010) at the Vacuum Tower Telescope (VTT; von der Lühe 1998). The dispersion of the Fe I $\lambda 1078.3$ nm and Si I $\lambda 1078.6$ nm spectra amounts to $2.19 \text{ pm pixel}^{-1}$. The map (10:00–10:38 UT) consists of 180 scan positions with a step size of $0''.36$. The image scale of $0''.175 \text{ pixel}^{-1}$ along the slit direction was resampled to $0''.35 \text{ pixel}^{-1}$ to reduce the noise in preparation for the spectral inversions. For each Stokes parameter, we accumulated ten exposures of 250 ms (see Balthasar & Gömöry 2008).

The Fe I and Si I lines sample different atmospheric layers of the quiet Sun, only in dark umbrae they originate at almost the same height (see Balthasar & Gömöry 2008). We derived the magnetic field vector using ‘Stokes inversions based on response functions’ (SIR; Ruiz Cobo & del Toro Iniesta 1992). The two lines were inverted separately. The magnetic field strength, the magnetic inclination and azimuth as well as the Doppler velocity were kept constant with height, whereas we use three nodes for the temperature. Initially, the magnetic azimuth ambiguity was

arXiv:1401.4386v1 [astro-ph.SR] 17 Jan 2014

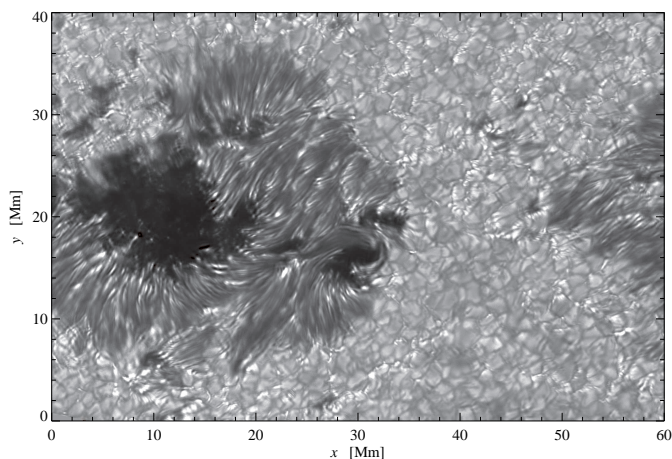


Fig. 1. G-band image of the δ -spot in active region NOAA 11504.

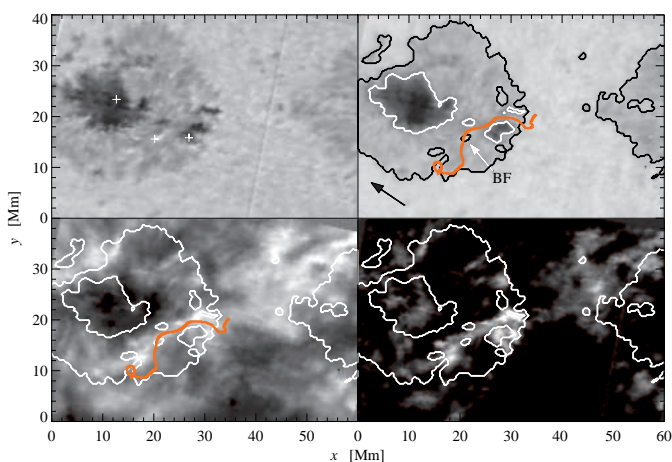


Fig. 2. Maps of continuum intensities at $\lambda 1078$ and $\lambda 854$ nm, Ca II $\lambda 854.2$ nm line-core intensity, and maximum of the central Ca II emission (top-left to bottom right). The ordinate is along the solar North-South direction. The black arrow points towards disk center, and the white arrow indicates the bright feature BF near the PIL (thick red line). Contour lines denote the umbral and penumbral boundaries. Three white crosses mark the positions of the spectral profiles in Fig. 3.

resolved by selecting directions matching a radial configuration with a common center (see Balthasar 2006). The subsequently applied minimum energy method of Leka et al. (2009) yields a more reliable configuration. Finally, we rotated the magnetic vector to the local reference frame and corrected the images for projection effects (see Verma et al. 2012). The resulting field-of-view (FOV) of $60 \text{ Mm} \times 40 \text{ Mm}$ served as a reference for all auxiliary data.

Multi-frame blind deconvolution (MFBD; van Noort et al. 2005) was applied to high-resolution ($0''.04 \text{ pixel}^{-1}$) G-band context images (see Fig. 1), which were recorded in the VTT’s optical laboratory. Additional Ca II $\lambda 854.2$ nm spectra with a dispersion of $0.82 \text{ pm pixel}^{-1}$ and an image scale of $0''.35 \text{ pixel}^{-1}$ were acquired at the Echelle spectrograph with a camera mounted next to TIP. Integration times of 9 s matched the TIP accumulation cycle. The spectral range also covered the Si I $\lambda 853.6$ nm line, which is weak and has a high excitation potential of 6.15 eV, thus, representing deep photospheric layers.

Magnetograms of the Helioseismic and Magnetic Imager (HMI; Schou et al. 2012) on board of the Solar Dynamics Ob-

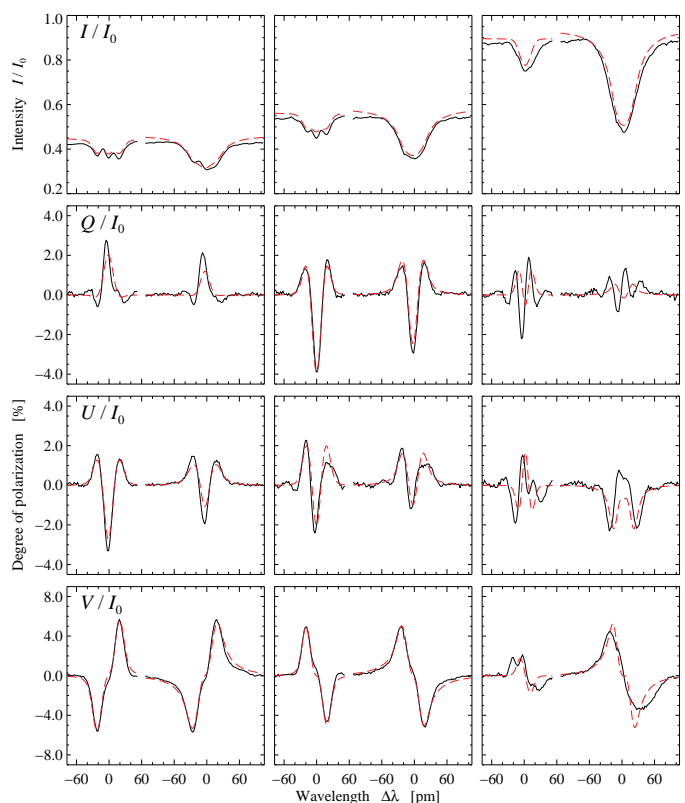


Fig. 3. Observed (solid) and inverted (dashed) Stokes-profiles in the umbra of the main spot (left), the δ -spot umbra (middle), and in the penumbra near BF (right). The wavelength is given with respect to the center of the Fe I $\lambda 1078.3$ nm (left) and Si I $\lambda 1078.6$ nm (right) lines, respectively. I_0 is the quiet-Sun continuum intensity at disk center.

servatory (SDO; Pesnell et al. 2012) accompany the VTT data and provide information of the magnetic field evolution and are used to determine horizontal velocities.

3. Results

Penumbral filaments related to the δ -umbra display a counter-clockwise twist in the central part of Fig. 1, while those of the main umbra show an opposite twist in the vicinity of the δ -umbra. The braided strands of penumbral filaments are parallel to the PIL and roughly perpendicular to the line connecting the centers of the main and δ -umbrae.

Figure 2 shows continuum intensity images at $\lambda 1078$ nm and $\lambda 854$ nm. Apart from the main umbra, several dark features reside in the common penumbra. Yet only one dark umbral core close to the right border of the penumbra at the location $(x, y) \sim (28, 15) \text{ Mm}$ possesses opposite magnetic polarity. Central emission of the Ca II line is mainly present in the δ -umbra and along a diagonal starting just to the north of the δ -umbra and extending for about 30 Mm to the south-east. We refer to this alignment of brightenings as ‘central emission line’ (CEL), which is in some locations, but not everywhere, co-spatial with the PIL. The CEL is inconspicuous in continuum images.

A comparison of observed and fitted Stokes-profiles for three selected pixels (marked in Fig. 2) is shown in Fig. 3. Observed and fitted profiles agree rather well for the main and the δ -umbra, but for a point on the PIL near the bright feature (BF) indicated in Fig. 2, a single-component inversion is not able to reproduce the observed multi-lobe profiles.

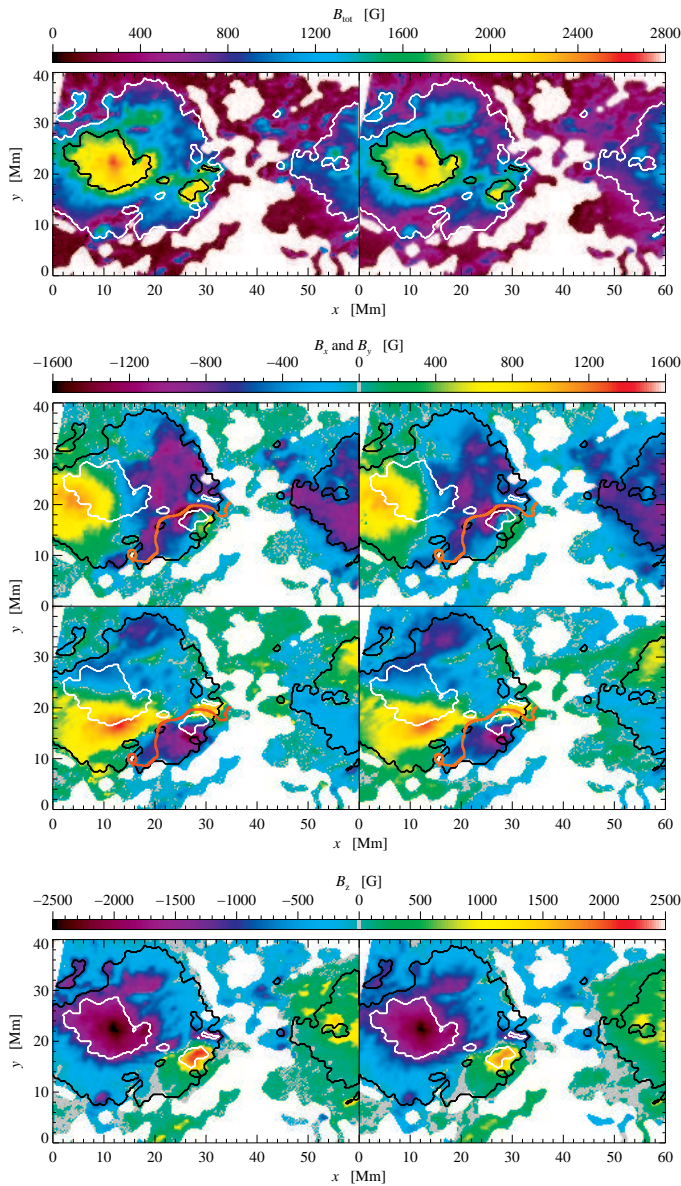


Fig. 4. Total magnetic field B_{tot} and Cartesian components B_x , B_y , and B_z (top to bottom) derived from inversions of the Fe I $\lambda 1078.3$ nm (left) and Si I $\lambda 1078.6$ nm (right) lines, respectively.

The total magnetic field strength $B_{\text{tot}} = |\mathbf{B}|$ and Cartesian components of the magnetic field vector $\mathbf{B} = (B_x, B_y, B_z)$ have been determined with SIR for the Fe I $\lambda 1078.3$ nm and Si I $\lambda 1078.6$ nm lines. The vertical component B_z in Fig. 4 reveals clearly the opposite polarities of the main and δ -umbrae. The parasitic polarity is positive like that of the leading sunspot in the active region. Inversions of the Fe I and Si I lines bring forth field strengths in the main umbra of up to 2600 G and 2570 G, respectively. Corresponding values in the δ -umbra reach only 2250 G and 2030 G. The height difference between the formation layers of the two NIR spectral lines is larger above the δ -umbra, because it is hotter than the main umbra. Nevertheless, dividing the difference in B_{tot} by the difference in height covered by the two lines (see Balthasar & G6m6ry 2008) indicates that the magnetic field decreases much faster with height in the δ -umbra as compared to the main umbra. In the δ -umbra, the mean formation height of the Fe I line is 150 km and that of the Si I line is 210 km. The corresponding values at the center of the main

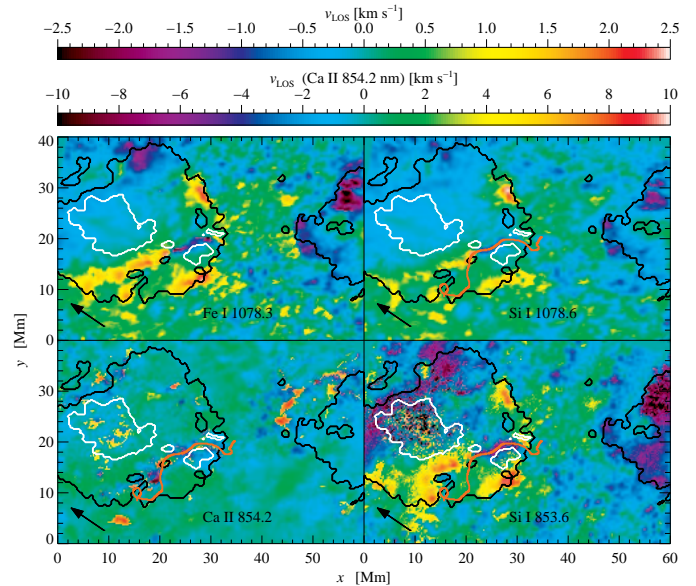


Fig. 5. Doppler velocities obtained with SIR (top) based on the Fe I $\lambda 1078.3$ nm (left) and Si I $\lambda 1078.6$ nm (right) lines, respectively. Line-fitting (bottom) yields LOS velocities of the chromospheric Ca II $\lambda 854.2$ nm (left) and photospheric Si I $\lambda 853.6$ nm (right) lines. Note the different scale bar for the velocities from the Ca II line.

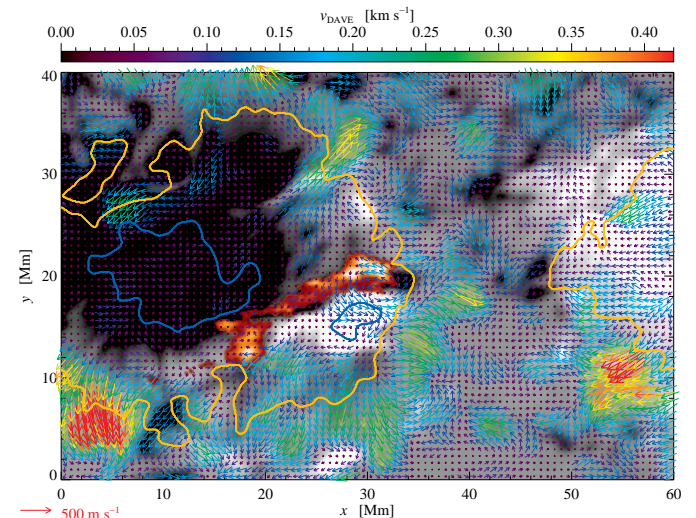


Fig. 6. One-hour averaged HMI magnetogram (clipped to ± 500 G in gray scale) with superimposed vectors of v_{DAVE} . Length (see arrow below the figure) and color of the vectors represent the magnitude of v_{DAVE} . Emission along the CEL is indicated by the red background.

umbra are 140 km and 180 km, respectively. With these values, we find magnetic gradients of $\Delta B_{\text{tot}}/\Delta z \approx 4.5 \pm 1.4 \text{ G km}^{-1}$ and $2 \pm 0.5 \text{ G km}^{-1}$, respectively. B_{tot} is rather low below the south-eastern part of the CEL.

B_x varies smoothly with negative values in the region between the two umbrae. The perpendicular component B_y has a positive sign south of the main umbra and north of the δ -umbra, whereas it is negative on the other side. In the northern part of the spot, these opposite signs are well separated, but in the southern part, at the edge of BF, large values of B_y with opposite signs occur in close proximity. Inside BF, B_z is positive. The PIL bends at BF and separates from the CEL. At these locations, anomalous multi-lobed Stokes-profiles arise (see right column in Fig. 3),

which cannot be reproduced by a single-component inversion. (A two-component inversion is beyond the scope of this Letter.) Changing the magnetic azimuth by 180° even compounds this problem. Lites et al. (2002) explained such profiles in terms of interleaved systems of magnetic field lines. Such interleaved systems might facilitate reconnections, but in our case, the region was small enough not to cause a major flare.

The Doppler velocities derived from different lines are summarized in Fig. 5. Photospheric lines exhibit the Evershed effect as blue-shifts in the upper left part of the spots and as red-shifts on the right side. The Evershed effect is most pronounced in the Si I $\lambda 853.6$ nm line that forms at deep layers. The Evershed flow from the main umbra is interrupted in proximity to the area where it reaches the CEL, and where the filaments coming from the main umbra end. Beyond this line, it drops and finally reaches another maximum at the outer edge of the penumbra. A strong blue-shift of about 1 km s^{-1} is apparent just to the north of the δ -umbra along the PIL. We cannot finally decide whether this blue-shift corresponds to an upflow or an Evershed-like flow away from the δ -umbra because the spot is at some distance from disk center. This blue-shift encompasses the PIL, where the magnetic field is horizontal, implying that the flow is more horizontal as well. The Evershed effect is also present in the Ca II $\lambda 854.2$ nm line. Patches of high velocities of up to 8 km s^{-1} exist along the CEL occurring both as blue-shifts and as red-shifts. High red-shifts appear also in the periphery of the spot (cf., Balthasar et al. 2013). Because these patches are small, we interpret them as vertical flows, in agreement with downflows found by Martínez Pillet et al. (1994), although we do not find supersonic flows in photospheric layers (see Takizawa et al. 2012).

The ‘differential affine velocity estimator’ (DAVE, Schuck 2005, 2006) estimates the magnetic flux transport velocity v_{DAVE} by utilizing an affine velocity profile and minimizing the deviation in the magnetic induction equation. The input HMI magnetograms have been aligned, corrected for geometrical foreshortening, and adjusted for the μ -dependence of the magnetic field strength assuming that the field lines are perpendicular to the solar surface. DAVE depends on the temporal derivative of the magnetograms implemented as a five-point stencil, spatial derivatives carried out with the Scharf (2007) operator, and a sampling window of prescribed size (11 pixels ~ 3520 km). Arrows overlaid on the magnetogram in Fig. 6 indicate the one-hour averaged (09:30–10:30 UT) v_{DAVE} in the δ -umbra’s neighborhood. The horizontal velocity structure differs from a regular sunspot. The most distinct velocity feature is a counterclockwise spiral motion centered between the δ -umbra and a neighboring dark feature. In addition, shear flows parallel to the CEL prevail locally with an imbalance of 0.2 km s^{-1} towards stronger flows on the δ -umbra side. This value compares to the 0.3 km s^{-1} found by Tan et al. (2009) after a flare. Denker et al. (2007) discussed that such velocities do not necessarily build up magnetic shear, and the observed drift does not destabilize the magnetic configuration. Between main and δ -umbra, v_{DAVE} amounts to 0.2 km s^{-1} and cross the PIL in the opposite direction as v_{LOS} .

The CEL seems to be of much higher importance for this spot than the PIL. An explanation could be that new bipolar flux emerged southwest of the main umbra, and the CEL separates the new flux from the pre-existing one. Between main and δ -umbra, PIL and CEL are identical, but then the PIL bends at BF and crosses the new bipolar flux. Such a scenario also explains that the Evershed flow related to the main umbra ends at the CEL. In the range of repelling field lines from the two flux systems, chromospheric brightenings occur as well as between attracting field lines.

4. Conclusions

The magnetic field strength B_{tot} at deep photospheric layers amounts to 2250 G in the δ -umbra, somewhat less than the 2600 G of the main umbra. It decreases twice as fast with height in the δ -umbra compared to the main umbra. We find a smooth transition of the magnetic vector field between the two umbrae of opposite polarity. At some distance from the δ -umbra, near BF, we find a discontinuity of the horizontal magnetic field due to an interleaved system of magnetic field lines.

The δ -umbra causes its own Evershed flow which is separated from that of the main umbra. Along the CEL, we find flows of $\pm 8 \text{ km s}^{-1}$ in chromospheric layers. We observe a horizontal flow of magnetic features (‘magnetic flux transport velocities’) on one side parallel to the CEL with an imbalance of 0.2 km s^{-1} . The magnetic configuration of the δ -spot is seemingly stable for at least 10 hours. The group produced an M1.9-flare on June 14 and several C-flares during the previous day, but no flare of class C or larger was recorded by the GOES satellite during 19 hours before and 6 hours after our observation.

The central emission patches in the Ca II line at 854.2 nm indicate that important physical processes happen in the chromospheric layers above δ -spots. For future observations, e.g. with the GREGOR Infrared Spectrograph (GRIS, Collados et al. 2012) at the GREGOR solar telescope (Schmidt et al. 2012), the chromospheric magnetic field should be investigated too, e.g., to search for probable current sheets.

Acknowledgements. We are grateful to L. Bellot Rubio for carefully reading the manuscript and his valuable comments. The VTT is operated by the Kiepenheuer-Institut für Sonnenphysik (Germany) at the Spanish Observatorio del Teide of the Instituto de Astrofísica de Canarias. SDO/HMI data are provided by the Joint Science Operations Center – Science Data Processing. MV expresses her gratitude for the generous financial support by the German Academic Exchange Service (DAAD) in the form of a PhD scholarship. CD and REL were supported by grant DE 787/3-1 of the German Science Foundation (DFG).

References

- Balthasar, H. 2006, A&A, 449, 1169
 Balthasar, H. & Gömöry, P. 2008, A&A, 488, 1085
 Balthasar, H., Beck, C., Gömöry, P., et al. 2013, *Centr. Europ. Astrophys. Bull.*, 37, 435
 Berkefeld, T., Soltau, D., Schmidt, D. & v. d. Lüche, O. 2010, *Appl. Opt.*, 49, G155
 Collados, M., Lagg, A., Díaz García, J. J., et al. 2007, in *ASP Conf. Ser.*, 368, The Physics of Chromospheric Plasmas, eds. P. Heinzel, I. Dorotovič & R. J. Rutten, 611
 Collados, M., López, R., Páez, E., et al. 2012, *AN*, 333, 872
 Denker, C., Deng, N., Tritschler, A. & Yurshyshyn, V. 2007, *Sol. Phys.*, 245, 219
 Fischer, C. E., Keller, C. U., Snik, F., et al. 2012, A&A, 547, A34
 Hürzberger, J., Riethmüller, T., Lagg, A., et al. 2009, A&A, 505, 771
 Jennings, D. E., Deming, D., McCabe, G., et al. 2002, *ApJ*, 568, 1043
 Künzel, H. 1960, *AN*, 285, 271
 Künzel, H. 1965, *AN*, 288, 177
 Leka, K. D., Barnes, G., Crouch, A. D., et al. 2009, *Sol. Phys.*, 260, 83
 Lites, B. W., Socas-Navarro, H., Skumanich, A. & Shimizu, T. 2002, *ApJ*, 575, 1131
 Martínez Pillet, V., Lites, B. W., Skumanich, A. & Degenhardt, D. 1994, *ApJ*, 425, L113
 Min, S. & Chae, J. 2009, *Sol. Phys.*, 258, 203
 Pesnell, W. D., Thompson, B. J. & Chamberlin, P. C. 2012, *Sol. Phys.*, 275, 3
 Ruiz Cobo, B. & del Toro Iniesta, J. C. 1992, *ApJ*, 398, 375
 Sammis, I., Tang, F. & Zirin, H. 2000, *ApJ*, 540, 583
 Scharf, H. 2007, in *LNCS*, 3417, *Complex Motion*, eds. D. Hutchison et al., 14
 Schmidt, W., von der Lüche, O., Volkmer, R., et al. 2012, *AN* 333, 796
 Schou, J., Scherrer, P. H., Bush, R. I., et al. 2012, *Sol. Phys.*, 275, 229
 Schuck, P. W. 2005, *ApJ*, 632, L53
 Schuck, P. W. 2006, *ApJ*, 646, 1358
 Takizawa, K., Kitai, R. & Zhang, Y. 2012, *Sol. Phys.* 281, 599
 Tan, C., Chen, P. F., Abramenko, V. & Wang, H. 2009, *ApJ*, 690, 1820
 v. Noort, M., Rouppe v. d. Voort, L. & Löfdahl, M. G. 2005, *Sol. Phys.*, 228, 191
 Verma, M., Balthasar, H., Deng, N., et al. 2012, A&A, 538, A109
 v. d. Lüche, O. 1998, *New Astron. Rev.*, 42, 493
 Xu, Y., Cao, W., Liu, C., et al. 2004, *ApJL*, 607, 131
 Xu, Y., Cao, W., Liu, C., et al. 2006, *ApJ*, 641, 1210